Dyes and Pigments 80 (2009) 11–16

Contents lists available at ScienceDirect

Dyes and Pigments

journal homepage: www.elsevier.com/locate/dyepig

The synthesis, crystal structure and photophysical properties of three novel naphthalimide dyes

Wei Jiang [a], Jinan Tang [a], Qi Qi [a], Weibing Wu [a], Yueming Sun [a,*], Dawei Fu [b]

[a] School of Chemistry and Chemical Engineering, Southeast University, Nanjing 210096, PR China
[b] Ordered Matter Science Research Center, College of Chemistry and Chemical Engineering, Southeast University, Nanjing 210096, PR China

ARTICLE INFO

Article history:
Received 5 March 2008
Received in revised form 5 April 2008
Accepted 14 April 2008
Available online 30 April 2008

Keywords:
Naphthalimide
Synthesis
Carbazole
Crystal structure
Photophysical
Charge-transfer

ABSTRACT

Three new naphthalimide derivatives containing an electron-donor moiety (carbazole), 4-carbazolyl-*N*-methyl-1,8-naphthalimide, 4-carbazolyl-*N*-cyclohexyl-1,8-naphthalimide and 4-carbazolyl-*N*-phenyl-1,8-naphthalimide were synthesized and crystal structures confirmed. Crystallographic data revealed that the interplanar angles (θ) of the carbazole and naphthalimide moieties were, respectively, 70.7° and 66.5°. The UV–vis absorption and photoluminescent spectra of the systems in *n*-hexane, $CHCl_3$, tetrahydrofuran and CH_2Cl_2 were investigated. The lowest absorption band of the naphthalimide molecular centered at 400–420 nm was assigned to charge-transfer transition with emission at ≈440 nm in *n*-hexane and at ≈560 nm in CH_2Cl_2.

1. Introduction

Aromatic systems with strong electron-donor and acceptor substituent groups often exhibit solvent-dependent emission properties due to internal charge-transfer (ICT) processes in the excited state. In the field of organic light-emitting diodes (OLED), carbazoles are ideal electron donors with high carrier mobility, high thermal and photochemical stabilities, and these properties are commonly used as hole-transporting materials for balanced charge injection and transport in LED devices [1,2]. On the other hand, naphthalimide is an excellent electron accepting chromophore, which has often been used for constructing materials for green or yellow light emission [3,4]. Naphthalimides comprise a class of fluorophore whose electronic absorption and emission depend upon the properties of the surrounding medium. The photophysical behavior of 1,8-naphthalimide derivatives is a function of C-4 substitution. Substitution of electron-donating groups usually increases the fluorescence emission, particularly when a methoxy or amino group at C-4 position is used. Thus, they have a wide range of applications as organic dyes and luminophore [5,6], probes for analytical purposes [7,8], fluorophores for optical chemosensing [9,10], laser dyes and liquid crystal displays [11,12].

Here, we report the study on the synthesis, crystal structure and photophysical properties of three new ICT compounds based on carbazole and naphthalimide units. The structures are shown in Scheme 1. The absorption and emission spectra are examined. The broad range of emissions may indicate the formation of a charge-transfer state. In the molecular structure, the carbazole and naphthalimide units twist with each other and act as an electron-donor while the naphthalimide unit acts as an electron-acceptor. In this work, the influence of solvents with various polarities upon absorption and emission spectra was investigated and the charge-transfer phenomenon in these compounds was systematically studied.

2. Experimental

2.1. General

Melting points were determined on a digital melting point apparatus WRS-1 made in shanghai and uncorrected. IR spectra were recorded on a 5DX-FT-2 spectrophotometer using KBr pellets. ^1H NMR and ^{13}C NMR spectra were recorded on Bruker (ARX-500) spectrophotometer (500 MHz) in $CDCl_3$ and using TMS as internal standard (chemical shift are given as δ in ppm). The mass spectra were recorded on ZAB-HS spectrometer. Elemental analyses were performed on Elementar Vario MICRO. UV–vis aborption spectra were recorded using a Hitachi U-300 spectrophotometer, while photoluminescent spectra were

* Corresponding author. Tel.: +86 25 52090619; fax: +86 25 52090621.
E-mail address: sun@seu.edu.cn (Y. Sun).

0143-7208/$ – see front matter © 2008 Elsevier Ltd. All rights reserved.
doi:10.1016/j.dyepig.2008.04.005

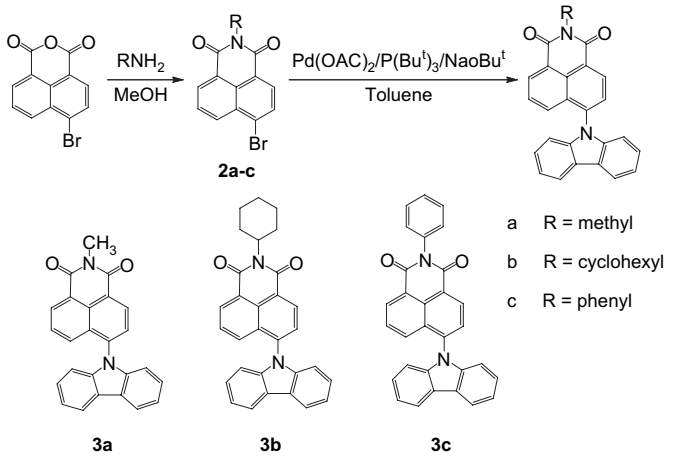

Scheme 1. Synthetic route of **3a**–**c**.

a Hitachi F-4050. The quantum yields for emission were measured at room temperature with fluorescein (in 0.1 M NaOH, quantum yield = 0.93) as the standard. All reactions were monitored by thin-layer chromatography. Common reagent grade chemicals are commercially available and were used without further purification.

2.2. Synthesis

The synthetic route was shown in Scheme 1. To a two-necked flask under nitrogen were added compounds **2a**–**c** (1 mmol), carbazole (1.2 mmol), $Pd(OAC)_2$ (0.020 mmol), tri-*tert*-butyl phosphine (0.04 mmol), and sodium *tert*-butoxide (1.5 mmol). Toluene (3 ml) was then added to the flask via a syringe. The resulting mixture was stirred for 4–6 h at 120 °C. After cooling, to the mixture was added water (3 ml) and then ethyl acetate (20 ml). The organic layer was separated from the aqueous layer, washed with water and brine solution, and dried over anhydrous magnesium sulfate. Evaporation of the solvent under reduced pressure afforded the crude solid. Purification on a silica gel column using a petroleum ether/ethyl acetate mixture as the eluent gave the desired pure products in >80% yields.

2.2.1. 4-Carbazolyl-N-*methyl*-1,8-naphthalimide (***3a***)

Yield: 90%; Mp: 185–186 °C; green powder; ^{1}H NMR (500 MHz, $CDCl_3$, TMS) δ: 8.88 (d, J = 7.6 Hz, 1H), 8.75 (d, J = 6.9 Hz, 1H), 8.28 (d, J = 7.0 Hz, 2H), 7.98 (d, J = 7.5 Hz, 1H), 7.87 (d, J = 8.3 Hz, 1H), 7.70 (t,

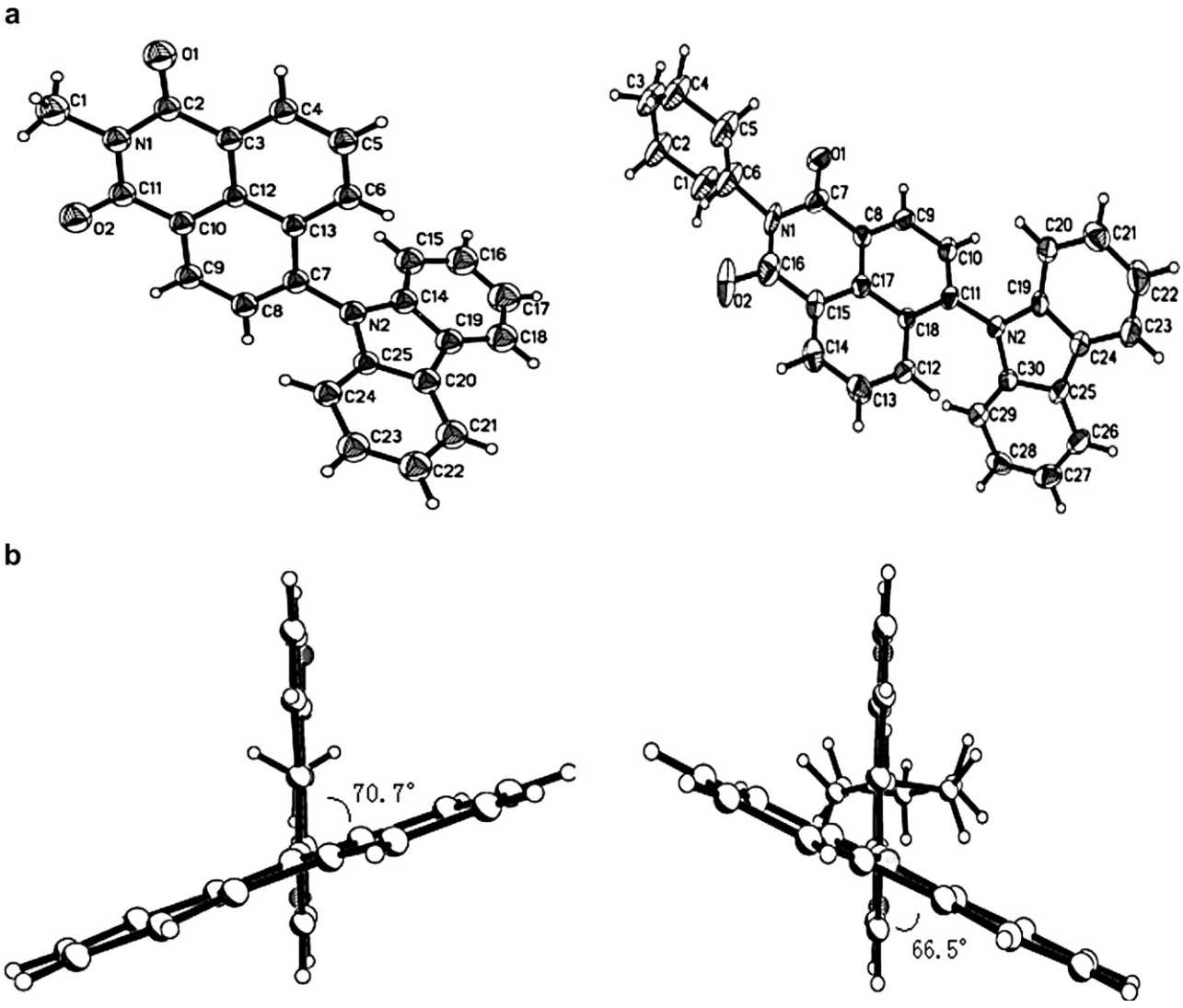

Fig. 1. (a) Ortep diagram of **3a** and **b**; (b) side view of **3a** and **b**.

$J = 7.4$, 8.2 Hz, 1H), 7.45–7.39 (m, 4H), 7.09 (d, $J = 7.6$ Hz, 2H), 3.69 (s, 3H); ^{13}C NMR($CDCl_3$): δ 164.26, 163.87, 141.71, 140.37, 132.04, 131.62, 130.24, 129.58, 129.02, 127.65, 127.36, 126.38, 123.77, 123.31, 122.60, 120.74, 120.61, 109.99, 27.21; IR (KBr, cm^{-1}) 1699, 1657, 1582, 1491, 1357, 1271, 754; MS (70 eV) m/z 376(M^+); Anal. calcd for $C_{25}H_{16}N_2O_2$: C, 79.79; H, 4.26; N, 7.45; found C, 79.65; H, 4.50; N, 7.55.

2.2.2. 4-Carbazolyl-N-cyclohexyl-1,8-naphthalimide (**3b**)

Yield: 85%; Mp: 235–236 °C; green powder; ^{1}H NMR (500 MHz, $CDCl_3$, TMS) δ: 8.83 (d, $J = 7.6$ Hz, 1H), 8.70 (d, $J = 7.1$ Hz, 1H), 8.28 (d, $J = 7.1$ Hz, 2H), 7.96 (d, $J = 7.6$ Hz, 1H), 7.82 (d, $J = 8.4$ Hz, 1H), 7.68 (t, $J = 7.7$, 7.9 Hz, 1H), 7.44–7.39 (m, 4H), 7.08 (d, $J = 7.5$ Hz, 2H), 5.17–5.12 (m, 1H), 2.70–2.62 (m, 2H), 2.00–1.98 (m, 2H), 1.87–1.80 (m, 3H), 1.59–1.53 (m, 2H), 1.45–1.41 (m, 1H); ^{13}C NMR($CDCl_3$): δ 164.42, 164.02, 141.70, 139.88, 139.44, 131.88, 131.47, 129.76, 129.70, 128.85, 127.66, 127.33, 126.36, 125.83, 123.99, 123.73, 123.34, 123.30, 120.68, 120.60, 120.34, 119.41, 110.58, 109.99, 53.98, 53.49, 29.15, 26.58, 25.47; IR (KBr, cm^{-1}) 1699, 1660, 1589, 1450, 1232, 750, 725; MS (70 eV) m/z 444(M^+); Anal. calcd for $C_{30}H_{24}N_2O_2$: C, 81.08; H, 5.40; N, 6.31. Found: C, 81.20; H, 5.40; N, 6.20.

2.2.3. 4-Carbazolyl-N-phenyl-1,8-naphthalimide (**3c**)

Yield: 82%; Mp: 218–219 °C; yellow powder; ^{1}H NMR (500 MHz, $CDCl_3$, TMS) δ: 8.92 (d, $J = 7.6$ Hz, 1H), 8.79 (d, $J = 7.1$ Hz, 1H), 8.30 (d, $J = 7.2$ Hz, 2H), 8.02 (d, $J = 7.6$ Hz, 1H), 7.93 (d, $J = 8.4$ Hz, 1H), 7.74 (t, $J = 7.8$ Hz, 1H), 7.67 (t, $J = 7.5$ Hz, 2H), 7.60 (t, $J = 7.2$ Hz, 1H), 7.47–7.41 (m, 6H), 7.12 (d, $J = 7.7$ Hz, 2H); ^{13}C NMR($CDCl_3$): δ 164.16, 163.75, 141.71, 140.68, 135.21, 132.46, 132.03, 130.55, 130.11, 129.53, 129.19, 128.92, 128.61, 127.76, 127.45, 126.43, 123.82, 123.55, 122.81, 120.81, 120.66, 109.99; IR (KBr, cm^{-1}) 1710, 1666, 1587, 1450, 1375, 1232, 752; MS (70 eV) m/z 438(M^+); Anal. calcd for $C_{30}H_{18}N_2O_2$: C, 82.19; H, 4.11; N, 6.39. Found: C, 82.20; H, 4.40; N, 6.36.

2.3. Crystallography

Suitable monocrystals of **3a** and **b** were obtained by slow evaporation of methanol solution. All the measurements were made on a MERCURY CCD diffractometer by the ω scan technique at room temperature using graphite-monochromated Mo Kα radiation. The structures were solved by direct methods and refined by full-matrix least-squares procedures on F^2 (SHELXL-97). All non-hydrogen atoms were refined anisotropically. Crystallographic data for the structures in this paper have been deposited with the Cambridge Crystallographic Data Centre as supplemental publications CCDC 668999 for **3a** and 668998 for **3b**. Copies of the data can be obtained, free of charge, on application to CCDC, 12 Union Road, Cambridge CB2 1EZ, UK (fax: +44 0 1223 336033 or e-mail: deposit@ccdc.cam.ac.uk).

3. Results and discussion

3.1. Synthesis

The preparation of **3a–c** is shown in Scheme 1. The starting compounds **2a–c** were synthesized according to methods previously described [13]. The reaction of 4-Br-1,8-naphthalic anhydride in 1:1 molar ratio with RNH_2 in boiling ethanol for 12 h gives **2a–c** in good yield. The target 1,8-naphthalimide derivatives **3a–c** were obtained by nucleophilic substitution of the bromine atom at position 4 with carbazole group under palladium-catalyzed condition in >80% yield [14–16].

3.2. Crystal structure analysis

X-ray diffraction crystal analysis provided the final evidence for the compounds **3a** and **b** (Fig. 1). For **3c**, it was difficult to obtain crystals for X-ray analysis. Its crystal parameters are listed in Table 1, and selected crystal data are given in Table 2. There are some differences in the crystalline structure of these two compounds. The space groups of the two molecules, **3a** and **b**, were *Cc* and *P*-1, respectively. Intermolecular hydrogen bonding C–H···O is both present in **3a** and **b** [O2···H15–C15, 2.522 Å in **3a** and O1···H29–C29, 2.486 Å in **3b**]. Furthermore, a T-type CH/π interaction was found between the hydrogen atom on C21 and carbazole ring with 2.691 Å in **3a** (Fig. 2). Additionally, the two molecules show some differences between them in the interplanar angles (θ) of carbazole and naphthalimide moieties: 70.7° for the molecule **3a**, 66.5° for the molecule **3b**.

Table 1
Crystal data and structure refinement for **3a** and **3b**

	3a	**3b**
Formula	$C_{25}H_{16}N_2O_2$	$C_{30}H_{24}N_2O_2$
FW	376.40	444.51
Crystal system	Monoclinic	Triclinic
Space group	*Cc*	*P*-1
a (Å)	10.747(11)	7.879(2)
b (Å)	27.46(2)	10.903(2)
c (Å)	7.330(7)	13.877(3)
α (°)	90	75.91(3)
β (°)	120.173(9)	83.81(3)
γ (°)	90	8.52(3)
Z	4	2
V	1870(3)	1130.9(4)
D_{calc} ($g\,cm^{-3}$)	1.337	1.305
T (K)	293(2)	293(2)
Radiation λ (Å)	Mo Kα (0.71073)	Mo Kα (0.71073)
μ (mm^{-1})	0.086	0.082
Reflections collected	7610	9402
Reflections observed	3277	3976
Number of parameters	308	279
Final $R1[I > 2\sigma(I)]$	0.0440	0.1123
$wR2[I > 2\sigma(I)]$	0.0986	0.1996
*R*1 (all data)	0.0532	0.2554
*wR*2 (all data)	0.0938	0.2353
Goodness-of-fit on *F*2	0.939	1.209

3.3. Photophysical properties

The fluorescence and absorption spectra of the naphthalimides **3a–c** have been studied in various solvents of different polarity and the spectral data have been collected in Table 3. A few representative spectra are shown in Figs. 3 and 4. As indicated in the

Table 2
Selected bond lengths and angles for **3a** and **3b**

Compound	Bond lengths (Å)	Bond angles (°)	
3a	N2–C23 = 1.392(4)	C23–N2–C24 = 124.4(2)	C1–N1–C13 = 125.4(2)
	N2–C24 = 1.388(3)	C23–N2–C25 = 118.0(2)	O2–C23–N2 = 120.2(2)
	N2–C25 = 1.470(3)	C24–N2–C25 = 117.6(2)	O2–C23–C16 = 122.1(3)
	C24–O1 = 1.228(3)	O1–C24–N2 = 119.9(2)	N2–C23–C16 = 117.6(2)
	N1–C12 = 1.396(3)	O1–C24–C18 = 122.4(2)	C14–C13–N1 = 119.3(2)
	N1–C1 = 1.404(3)	N2–C24–C18 = 117.7(2)	C22–C13–N1 = 119.6(2)
	N1–C13 = 1.432(3)	C12–N1–C1 = 109.0(2)	N1–C12–C11 = 129.9(2)
	C23–O2 = 1.226(3)	C12–N1–C13 = 125.5(2)	N1–C12–C7 = 107.8(2)
3b	N2–C1 = 1.385(6)	C1–N2–C12 = 108.5(5)	C24–N1–C25 = 114.9(7)
	N2–C12 = 1.397(6)	C1–N2–C13 = 124.3(5)	O2–C24–N1 = 123.7(7)
	N2–C13 = 1.426(6)	C12–N2–C13 = 127.1(5)	O2–C24–C20 = 118.9(7)
	O1–C23 = 1.211(7)	O1–C23–N1 = 118.3(7)	N2–C1–C6 = 108.8(5)
	N1–C23 = 1.413(8)	O1–C23–C18 = 124.3(8)	C26–C25–N1 = 119.3(5)
	N1–C24 = 1.396(8)	C2–C1–N2 = 129.8(5)	C30–C25–N1 = 115.5(5)
	N1–C25 = 1.488(7)	C23–N1–C24 = 123.9(6)	N1–C24–C20 = 117.3(6)
	O2–C24 = 1.225(7)	C23–N1–C25 = 120.9(6)	N1–C23–C18 = 117.3(7)

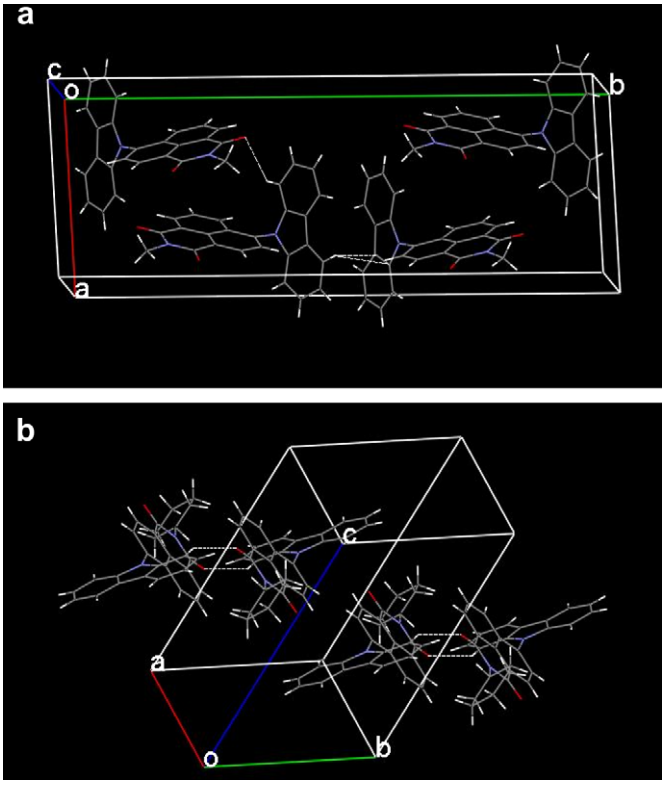

Fig. 2. Stereoview of crystal packing of **3a** (a) and **3b** (b).

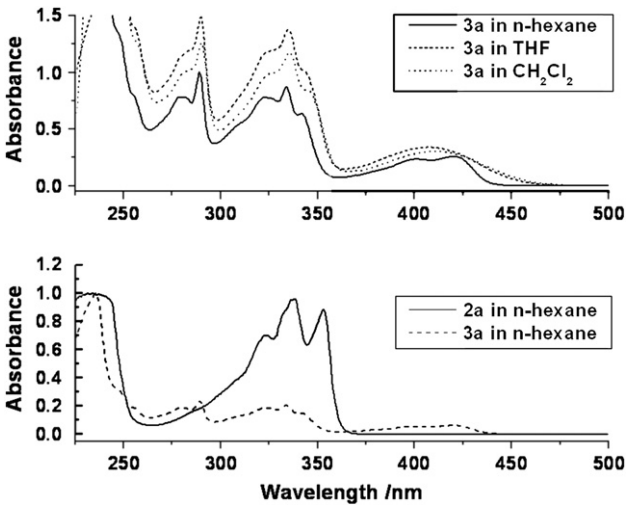

Fig. 3. Absorption spectra of **2a** in *n*-hexane and **3a** in *n*-hexane, THF and CH_2Cl_2.

absorption spectra, the vibrational structure of long-wavelength band in the absorption spectra is more clearly in *n*-hexane than in other more polar solvents. These derivatives reveal a common low-energy broad band at 400–420 nm assigned to an intramolecular charge-transfer (CT) band from the carbazole group to the naphthalimide ring system in all solvents. This is evident from the following observations: 4-non-amino substituted naphthalimides do not exhibit this band (vide Fig. 3), and other 1,8-naphthalimides which possess an electron-donating group at 4-position, display a similar band [17–19]; the absorption is fairly board and the peak position is rather sensitive to the polarity of the medium (vide Table 3).

Table 3 also listed fluorescence maximum emission in various solvents of different polarity. The fluorescence spectra of the systems consist of one broad band except in *n*-hexane, where some of the fine structure could be observed in *n*-hexane. The spectra of **3a**–**c** show a large Stokes shift in more polar solvents, accompanied by losing of the fine structure and an increase in the fluorescence half-width. As an example, the normalized fluorescence spectrum of **3a** is shown in Fig. 4. As a change of the solvent from *n*-hexane to CH_2Cl_2, the maximum emission wavelengths were red-shifted from 440 to 556 nm for **3a**. The Stocks shifts for **3a**–**c** are very large in polar solvents as compared to non-polar solvents indicating a considerable energetic stabilization of the excited state in polar solvents [20,21]. This finding, together with the UV–vis absorption data, clearly indicated that the absolute values of the excited state dipole moments are much higher than those of the ground state.

3.4. Measurement of the magnitude of the change in the dipole moment

The solvent dependence of the fluorescence indicates that the excited state is stabilized in more polar solvents, as expected for an intramolecular CT. In order to confirm this we used Reichart's solvent parameter $E_T(30)$ and $f(\varepsilon, n)$ solvent parameter and compared with Stokes shifts [22]. The variation of Stokes shift with solvent

Table 3
Maxima of UV absorption (λ^{abs}_{max}, nm), fluorescence maximum emission (λ^{PL}_{max}, nm), stokes shifts ($\Delta\nu_{st}$) and quantum yields for fluorescence (ϕ_f) of **3a**–**c** in different solvents at room temperature[a]

Compound	Solvent	$\Delta_f/E_T(30)$	λ^{abs}_{max} (nm)	ν_{abs} (cm^{-1})[b]	λ^{PL}_{max} (nm)	ν_{fl} (cm^{-1})[b]	$\Delta\nu_{st}$ (cm^{-1})[b]	ϕ_f[c]
3a	*n*-Hexane	0.001/30.9	402	24,875	440	22,727	2,148	0.895
	$CHCl_3$	0.148/39.1	404	24,752	489	20,437	4,315	0.204
	THF	0.207/37.4	408	24,509	537	18,621	5,888	0.031
	CH_2Cl_2	0.218/41.1	414	24,154	556	17,985	6,169	0.029
3b	*n*-Hexane	0.001/30.9	399	25,062	441	22,675	2,387	0.872
	$CHCl_3$	0.148/39.1	402	24,875	495	20,200	4,675	0.210
	THF	0.207/37.4	407	24,570	546	18,315	6,255	0.033
	CH_2Cl_2	0.218/41.1	410	24,390	563	17,761	6,629	0.030
3c	*n*-Hexane	0.001/30.9	403	24,813	443	22,573	2,240	0.887
	$CHCl_3$	0.148/39.1	405	24,691	495	20,183	4,508	0.198
	THF	0.207/37.4	408	24,509	546	18,315	6,194	0.032
	CH_2Cl_2	0.218/41.1	419	23,866	568	17,605	6,261	0.032

[a] Emission spectra were measured after exciting the solutions at the respective absorption maxima.
[b] $\nu_{abs} = 1/\lambda^{abs}_{max}$, $\nu_{fl} = 1/\lambda^{PL}_{max}$, $\Delta\nu_{st} = \Delta\nu_{abs-}\nu_{fl}$.
[c] With a measurement error of ±10%.

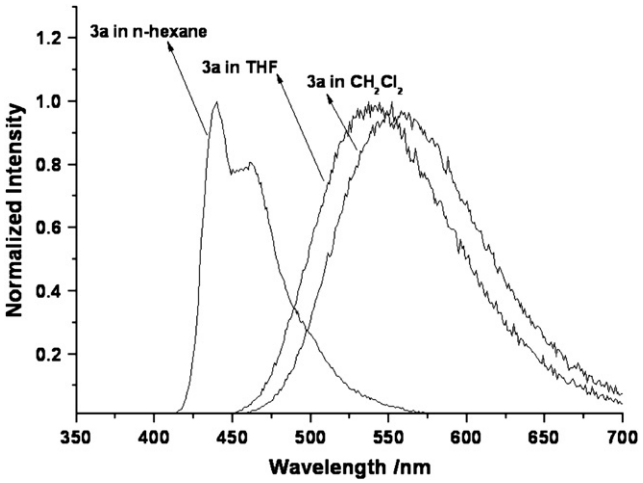

Fig. 4. Fluorescence spectra of **3a** in *n*-hexane, THF and CH_2Cl_2.

polarity can be represented by the Lippert–Mataga equation Eq. (1) [23,24].

$$\nu_a - \nu_f = 2\left[\Delta\mu^2/hca^3\right]\Delta f(\varepsilon, n) + C = 10070\left[\Delta\mu^2/a^3\right]\Delta f(\varepsilon, n) + C \quad (1)$$

where $\Delta f(\varepsilon, n)$ is calculated from Eq. (2):

$$\Delta f(\varepsilon, n) = [(\varepsilon - 1)/(2\varepsilon + 1)] - \left[\left(n^2 - 1\right)/\left(2n^2 + 1\right)\right] \quad (2)$$

and

$$a = (3M/4N\pi d)^{1/3} \quad (3)$$

In these relations, $\nu_a - \nu_f$ represents the Stokes shift (in cm^{-1}), where ν_a and ν_f are the spectral positions of the absorption maximum and solvent-equilibrated fluorescent maximum, respectively. $\Delta\mu$ is given by $\mu_e - \mu_g$, which is the magnitude of the change in the dipole moment from the ground state to the excited state. The other terms are: h corresponds to the Plank's constant (6.6×10^{-34} J s), c is the velocity of light in the vacuum (3.0×10^8 m s^{-1}) and a is the Onsager cavity radius (in meter), respectively. Onsager cavity radius was estimated from the optimized distance between the two farthest atoms in the direction of charge separation within the molecules, which was derived from the Avogadro number (N), molecular weight (M), and density (d). Δf is the orientation polarizability parameter of the solvent where n is the refractive index of the medium and ε is the static dielectric constant of the solvent (both at room temperature). The Lippert–Mataga plot for **3a–c** is shown in Fig. 5. From the slope of this plot, the difference of the dipole moment between the excited state and the ground state is estimated to be 15.83, 17.91 and 17.93 D for **3a–c**, respectively. This large change in dipole moment upon excitation is typical for photoinduced intramolecular CT processes.

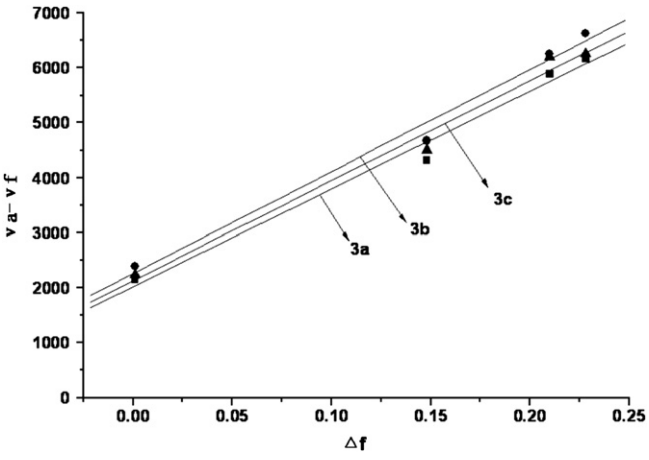

Fig. 5. Lippert–Mataga plot for **3a–c**.

4. Conclusions

In summary, three ICT compounds containing naphthalimide and carbazoles groups were synthesized using a palladium-catalyzed reaction and crystal structures of two compounds **3a** and **b** were determined. In addition the electronic absorption, fluorescence emission and photoinduced ICT behavior have been investigated. The results indicated that these dyes were strongly dependent on solvents and show generally bathochromic shifts as the polarity of solvents was increased. The dipole moment between the excited state and the ground state is estimated and the large change in dipole moment upon excitation is typical for photoinduced ICT processes.

Acknowledgements

The support of this research by the National 973 Fund (2007CB936300) and the High-Technique Project Foundation of Jiangsu Province (BG 2005034) is gratefully acknowledged.

References

[1] Justin TKR, Lin JT, Tao YT, Chuen CH. New carbazole–oxadiazole dyads for electroluminescent devices: influence of acceptor substituents on luminescent and thermal properties. Chemistry of Materials 2004;16:5437–44.
[2] Justin TKR, Lin JT, Tao YT, Ko CW. Light-emitting carbazole derivatives: potential electroluminescent matreials. Journal of American Chemical Society 2001;123:9404–11.
[3] Bojinov VB, Panova IP. Synthesis and absorption properties of new yellow-green emitting benzo[*de*]isoquinoline-1,3-diones containing hindered amine and 2-hydroxyphenylbenzotriazole fragments. Dyes and Pigments 2007;74:551–60.
[4] Grabtchev I, Philipova T, Meallier P. Influence of substituents on the spectroscopic and photochemical properties of naphthalimide derivatives. Dyes and Pigments 1996;31:31–4.
[5] Stewart WW. Lucifer dyes – highly fluorescent dyes for biological tracing. Nature 1981;292:17–21.
[6] Konstantinova TN, Meallier P, Grabtchev I. The synthesis of some 1,8-naphthalic anhydride derivatives as dyes for polymeric materials. Dyes and Pigments 1993;22:191–8.
[7] Hodgkiss RJ, Jones GW, Long A, Middleton RW, Parrick J, Stratfod MRL. Fluorescent markers for hypoxic cells: a study of nitroaromatic compounds, with fluorescent heterocyclic side chains, that undergo bioreductive binding. Journal of Medical Chemistry 1991;34:2268–74.
[8] Bailly C, Brana M, Waring M. Sequence-selective intercalation of antitumour bis-naphthalimides into DNA. European Journal of Biochemistry 1996;240:195–208.
[9] Rideout D, Schinazi R, Pauza CD, Lovelace K, Chiang LC, McCarthy M, et al. Derivatives of 4-amino-3,6-disulfonato-1,8-naphthalimide inhibit reverse transcriptase and suppress human and feline immunodeficiency virus expression in cultured cells. Journal of Cellular Biochemistry 1993;51:446–57.
[10] DeSilva AP, Gunaratne HQN, Habib-Jiwan JL, McCoy CP, Rice TE, Soumilion JP. New fluorescent model compounds for the study of photoinduced electron transfer: the influence of a molecular electric field in the excited state. Angewandte Chemie International Edition in English 1995;34:1728–31.
[11] Pardo A, Martin E, Poyato JML, Camacho JJ, Guerra JM, Weigand R, et al. *N*-substituted 1,8-naphthalimide derivatives as high efficiency laser dyes. Journal of Photochemistry and Photobiology A: Chemistry 1989;48:259–63.
[12] Martynski T, Mykowska K, Bauman D. Spectral properties of fluorescent dyes in nematic liquid crystals. Journal of Molecular Structure 1994;325:161–7.
[13] Alexiou MS, Tychopoulos V, Ghorbanian S, Tyman JHP, Brown RG, Brittain PI. The UV–visible absorption and fluorescence of some substituted 1,8-naphthalimides and naphthalic anhydrides. Journal of Chemical Society Perkin Transition 1990;2(12):837–42.

[14] Yamamoto T, Nishiyama M. Palladium-catalyzed synthesis of triarylamines from aryl halides and diarylamines. Tetrahedron Letters 1998;39:2367–70.
[15] Stieter ER, Blackmond DG, Buchwald SL. Insights into the origin of high activity and stability of catalysts derived from bulky, electron-rich monophosphinobiaryl ligands in the Pd-catalyzed C–N bond formation. Journal of American Chemical Society 2003;125:13978–90.
[16] Hooper MW, Utsunomiya M, Hartwig JF. Scope and mechanism of palladium-catalyzed amination of five-membered heterocyclic halides. Journal of Organic Chemistry 2003;68:2861–73.
[17] Elbrt JE, Paulsen S, Robinson L, Elzey S. Surface reaction of organic materials by laser ablation of matrix-isolated photoreactive aromatic azido compound. Journal of Photochemistry and Photobiology A: Chemistry 2005;169:9–19.
[18] Yuan DW, Brown RG. Enhanced nonradiative decay in aqueous solutions of aminonaphthalimide derivatives via water-cluster formation. Journal of Physical Chemistry A 1997;101:3461–6.
[19] Khosravi A, Moradian S, Gharanjig K, Taromi FA. Synthesis and spectroscopic studies of some naphthalimide based disperse azo dyestuffs for the dyeing of polyester fibres. Dyes and Pigments 2006;69:79–92.
[20] Jaung JY. Synthesis of new porphyrins with dicyanopyrazine moiety and their optical properties. Dyes and Pigments 2007;72:315–21.
[21] Jiang W, Sun YM, Wang XL, Wang Q, Xu WL. Synthesis and photochemical properties of novel 4-diarylamine-1,8-naphthalimide derivatives. Dyes and Pigments 2008;77:125–8.
[22] Reichardt C. Empirical parameters of solvent polarity as linear free-energy relationships. Angewandte Chemie International Edition in English 1979;18:98–110.
[23] Sumalekshmy S, Gopidas KR. Photoinduced intramolecular charge transfer in donor–acceptor substituted tetrahydropyrenes. Journal of Physical Chemistry B 2004;108:3705–12.
[24] Mataga N, Kaifu Y, Koizumi M. Solvent effects upon fluorescence spectra and the dipolemoments of excited molecules. Bulletin of the Chemical Society of Japan 1956;29:465–71.